BNL-213814-2020-JAAM

Reversible oxidation and reduction of gold-supported iron oxide islands at room temperature

Y. Jiang, D. Stacchiola

To be published in "The Journal of Chemical Physics"

February 2020

Center for Functional Nanomaterials

Brookhaven National Laboratory

U.S. Department of Energy

USDOE Office of Science (SC), Basic Energy Sciences (BES) (SC-22)

Notice: This manuscript has been authored by employees of Brookhaven Science Associates, LLC under Contract No. DE-SC0012704 with the U.S. Department of Energy. The publisher by accepting the manuscript for publication acknowledges that the United States Government retains a non-exclusive, paid-up, irrevocable, world-wide license to publish or reproduce the published form of this manuscript, or allow others to do so, for United States Government purposes.

DISCLAIMER

This report was prepared as an account of work sponsored by an agency of the United States Government. Neither the United States Government nor any agency thereof, nor any of their employees, nor any of their contractors, subcontractors, or their employees, makes any warranty, express or implied, or assumes any legal liability or responsibility for the accuracy, completeness, or any third party's use or the results of such use of any information, apparatus, product, or process disclosed, or represents that its use would not infringe privately owned rights. Reference herein to any specific commercial product, process, or service by trade name, trademark, manufacturer, or otherwise, does not necessarily constitute or imply its endorsement, recommendation, or favoring by the United States Government or any agency thereof or its contractors or subcontractors. The views and opinions of authors expressed herein do not necessarily state or reflect those of the United States Government or any agency thereof.

Reversible Oxidation and Reduction of Gold-supported Iron Oxide islands at Room Temperature

Yixuan Jiang[1,a], Yaguang Zhu[2,3,a], Dechun Zhou[1], Zhao Jiang[4,b], Nan Si[1], Dario Stacchiola[2,b], Tianchao Niu[1,b]

[1] Herbert Gleiter Institute of Nanoscience, School of Materials Science and Engineering, Nanjing University f Science & Technology, No. 200, Xiaolingwei, 210094, China
[2] Center for Functional Nanomaterials, Brookhaven National Laboratory, P.O. Box 5000, Upton, NY 11973-5000, USA
[3] Department of Mechanical Engineering & Materials Science and Engineering Program, State University of New York, Binghamton, New York 13902, United States
[4] Department of Chemical Engineering, Xi'an Jiaotong University, Xi'an, 710049, China

a) Contribution: Y. Jiang and Y. Zhu contributed equally to this work.
b) Electronic mail: J. Z. (jiangzhao@mail.xjtu.edu.cn); D. S. (djs@bnl.gov) and T. N. (tcniu@njust.edu.cn)

ABSTRACT

Monolayer iron oxides grown on metal substrates have been widely used as model systems in heterogeneous catalysis. By means of ambient-pressure scanning tunneling microscopy (AP-STM), we studied the *in situ* oxidation and reduction of FeO(111) grown on Au(111) by oxygen (O_2) and carbon monoxide (CO), respectively. Oxygen dislocation lines present on FeO islands are highly active for O_2 dissociation. X-ray photoelectron spectroscopy (XPS) measurements distinctly reveal the reversible oxidation and reduction of FeO islands after sequential exposure to O_2 and CO. Our AP-STM results show that excess O atoms can be further incorporated on dislocation lines and react with CO, whereas the CO is not strong enough to reduce the FeO supported on Au(111) that is essential to retain the activity of oxygen dislocation lines.

I. INTRODUCTION

Ultrathin oxide films on metal substrates show substantial differences in their physical and chemical properties compared with their bulk counterparts[1,2,3]. This phenomenon brings out the concept to design inverse oxide/metal catalysts that benefit from the strong oxide-metal interactions (SOMIs)[4,5]. Elegant examples include iron oxide[6,7], cobalt oxide[8,9], molybdenum oxide[10], silica[11,12], titania and ceria[13] on well-defined metal substrates[14]. Among these, iron oxide is one of the extensively explored systems because of its potential application in water-gas-shift reactions[15,16] and carbon monoxide (CO) oxidation[17,18]. For example, key elements for CO oxidation are the active sites to dissociate oxygen[19,20,21] and to anchor CO, which facilitate the interaction of CO with weakly bonded oxygen to form CO_2[22]. Many reaction pathways have been proposed based on combined surface science characterization tools and density functional theoretical (DFT) calculations, including the Langmuir-Hinshelwood type[23] and Mars-van Krevelen (MvK, creating a surface oxygen vacancy)[24,25] mechanisms. It is commonly accepted that the oxide/metal interfacial sites are more active than the terraces. According to the preparation and characterization of a series of FeO(111)/Pt(111) films with different island sizes, Fu *et al.* addressed that the reactivity of CO oxidation increases as a function of the periphery density. Based on DFT calculations, they found that both coordinatively unsaturated ferrous (CUF) sites at the oxide/metal interface and neighboring Pt atoms are the active centers, with the former one to activate oxygen, and Pt to anchor CO[26]. The active sites have been directly demonstrated by a high-resolution scanning tunneling microscopy (STM) study[27,28,29].

Oxygen activation is the crucial step in CO oxidation[19,21,30]. A variety of mechanisms were proposed, such as the formation of oxygen vacancy[31,32], and the assistance of hydroxyl group in the presence of water[33,34,35,36]. Most of these models emphasize the importance of boundaries between oxide and metal supports, or metal particles on oxide supports where the lattice oxygen can react directly with CO. Therefore, the generation of oxygen vacancies on the surface of oxide is one crucial step in CO oxidation. Bilayer FeO films were found to form a trilayer O-Fe-O film,

where CO can react with the top-surface oxygen forming CO_2 and leaving surface oxygen vacancy that will be replenished through the reaction with gas-phase oxygen[37]. In the absence of oxygen, oxidized FeO_{2-x} on Pt(111) is also active for the oxidation of CO which takes place at the interface between reduced and oxidized phases in the oxide thin film (400-450 K). It is the Pt substrate that promotes the formation of active interface, while the FeO_{2-x} with extra oxygen is essential for providing lattice oxygen to react with CO[38]. However, this catalyst barely can be regenerated even in oxygen rich conditions.

Reaction of CO with O_2 can produce carbonates on oxide surfaces[39,40], while the possible reduction of FeO_x to Fe by CO generates FeC_x[41]. These species are regarded as poisons that deactivate the catalysts[42]. Preparing appropriate catalysts with high efficiency and stability,[43] and optimizing reaction conditions are necessary to avoid deactivation. As the catalytic pathways and active sites depend on the pressure and temperature[44], it is imperative to monitor the atomic and chemical structures of catalysts under reaction conditions[45,46,47]. The developments of ambient-pressure surface science techniques, such as ambient-pressure STM (AP-STM)[48,49], and ambient-pressure X-ray photoelectron spectroscopy (AP-XPS)[50,20,21] have made it possible to bridge the pressure and temperature gap between traditional surface science studies in ultra-high vacuum (UHV) or low temperature and studies under reaction conditions[51].

Here, we use AP-STM to study the oxidation and reduction of FeO islands supported on Au(111) in O_2 and CO, respectively. The fresh FeO(111) surface comprising oxygen dislocation lines shows no obvious activity towards 1.5 mbar CO exposure at room temperature (RT). A large number of O atoms can be incorporated after exposing to 10^{-2} mbar O_2 gas that leads to the disappearance of dislocation lines on FeO(111) surface. Moreover, these dislocation lines are regenerated in 1.5 mbar CO gas. XPS measurements of Fe 2*p* and O 1*s* reveal the reversible oxidation and reduction of FeO islands after exposing to O_2 and CO, respectively. Control experiments by sequential exposing FeO islands to O_2 and CO show that the dislocation lines can be regenerated by exposing in 10^{-2} mbar O_2. In present study, *in situ* AP-STM results allow us to distinguish the stability of iron oxide and the crucial role of surface O species in

determining the reactivity.

II. METHODS

A. Sample preparation. Au(111) was cleaned by several cycles of Ar^+ sputtering (1.0 keV, 15 min) and annealing (800 K, 10 min). Monolayer FeO islands were prepared using the method reported in Ref. 41 by evaporating iron atoms in 1.5×10^{-7} mbar O_2 at 300 K followed by annealing at 600 K for 5min, and cooling down to 300 K in O_2 gas.

B. Surface Science Studies. Both AP-STM and XPS were attached to the preparation chamber, which allowed the sample transfer within UHV.

AP-STM measurements were performed at 300 K in batch mode with a commercial Leiden Probe Reactor STM setup [52]. The reactor cell is sealed by an inert fluoroelastomer ring, which allows switching the reactor cell between high-pressure (several bars) to UHV ($\sim10^{-8}$ mbar). All of the STM images were acquired in the constant-current mode with a top-to-down scan direction[53]. The scanning parameters are indicated in the figure captions.

Low-temperature UHV STM measurements were performed at 77K using a SPECS JT-SPM interfaced with a Nanonis controller. The sample was imaged in constant current mode using an electrochemically etched W tip.

XPS experiments were performed in a separated UHV chamber at a base pressure better than 2×10^{-10} mbar. The XPS (SPECS) was operated using an Al Kα photon source (1486.6 eV) and hemispherical electron analyzer set to a constant pass energy of 50 eV. Spectra were shifted to align the Au $4f_{7/2}$ peak to a binding energy of 84.0 eV. The presented XPS data have a step size of 0.05 eV and Shirley background subtractions have been applied. All of the spectra were recorded at 300 K.

C. DFT Calculations

DFT calculations were carried using the code Cambridge Sequential Total Energy Package (CASTEP) of Materials Studio[54]. A plane-wave cutoff energy of 400 eV is used to describe the electronic wave functions. The Perdew-Burke-Ernzerhof (PBE) functional with the generalized gradient approximation (GGA) was used to deal with the exchange-correlation energies[55]. The Brillouin-zone integration was performed by a 4×4×1 Monkhorst-Pack grid. For FeO (111) surface, O-terminated surface was

selected and modeled with a four-layer 2×2 super-cell (four Fe layers and four O layers) with the coverage of selected adsorbates of 1/4 monolayer. The Hubbard-U method was applied for the 3*d*-electrons of Fe atoms[56]. U = 5 eV was used for Fe ions to explore the correlation effects in 3*d* orbitals. Spin-polarization was considered for all calculations. The adsorbates and upper two layers are relaxed during all the optimization, while other layers are fixed. A vacuum layer of 15 Å is added along the direction perpendicular to the slab to avoid artificial interactions between the slab and its periodic images. The convergence criteria for configuration optimization is set to the tolerance for SCF, energy, maximum force, with a maximum displacement of 2.0×10^{-6} eV/atom, 2.0×10^{-5} eV/atom, 0.05 eV/ Å and 2.0×10^{-3} Å.

Au(111) is inert to both the CO and O_2 dissociation, and it acts as a support for the formation of FeO thin film. The coordinatively unsaturated sites of FeO on metal surfaces and the critical role of strong oxide-metal interactions in CO oxidation have been extensively explored[4,6,14]. In current studies, we mainly focused on the CO reactions with the activated O atoms on the FeO terrace, so we use FeO(111) only without considering the substrate in our calculations. According to our STM and XPS experiments, the oxygen dissociated along the dislocation lines to generate active oxygen atoms. Therefore, it is reasonable to simplify the model by using an individual O atom on the FeO(111) surface to stress the effect of these pre-adsorbed O atoms on CO oxidation.

The transition states (TS) are searched by complete Linear Synchronous Transit (LST) and Quadratic Synchronous Transit (QST) methods[57]. Furthermore, frequency analysis has been employed to ensure the TS with only one imaginary frequency. TS confirmation is made to ensure it leads to the desired reactant and product[53].

The adsorption energies on the FeO(111) surface are defined as:

$$E_{ads} = E_{adsorbate} + E_{slab} - E_{adsorbate/slab} \quad (1)$$

Where $E_{adsorbate/slab}$, $E_{adsorbate}$ and E_{slab} are the total energy of the surface with the adsorbate, the energy of the adsorbate and the energy of the surface.

For a reaction such as AB→A + B, the reaction energy (ΔH) and energy barrier (E_b) were calculated on the basis of the following formulas:

$$\Delta H = E_{(A+B)/surface} - E_{AB/surface} \quad (2)$$

$$E_b = E_{TS/surface} - E_{AB/surface} \quad (3)$$

where $E_{(AB)/surface}$ is the total energy of the adsorbed AB, $E_{(A+B)/surface}$ is the total energy of the co-adsorbed A/B on the metal surface, and the $E_{TS/surface}$ is the total energy of the transition state on the metal surface.

III. RESULTS AND DISCUSSION

A. CO and O_2 on FeO(111)

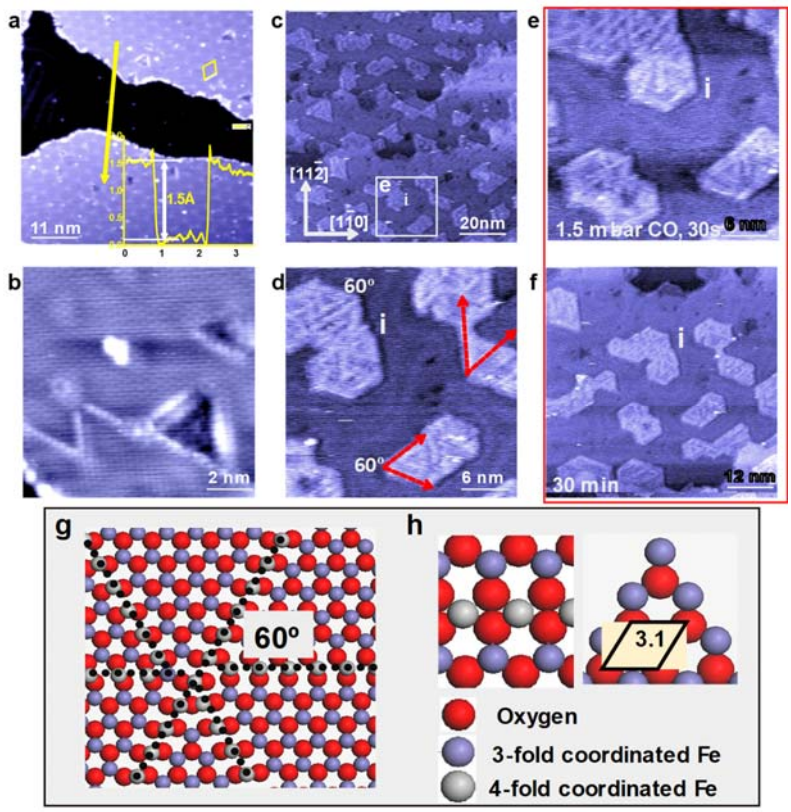

FIG. 1. FeO islands on Au(111). (a) LT-STM image of freshly prepared 0.8 ML FeO(111) on Au(111). Inset is a line-scan profile along the arrow across two domains; (b) Enlarged LT-STM image showing dislocation lines; (c) Freshly prepared FeO(111) with dislocation lines, image taken with AP-STM in UHV; (d) Zoomed image taken from the square in c. The arrows indicate the directions of the dislocation lines with an angle of 60º; (e) Same region during exposure to 1.5 mbar of CO; (f) large-scale image of FeO islands taken in 1.5 mbar CO; (g) Proposed ball model showing the dislocation lines that are composed of 4-fold coordinated Fe atoms. The structure is based on previous experiments and theory[27,64,65,]. (h) Enlarged model showing the 3-fold and 4-fold coordinated Fe atoms. Scanning parameters for (a) and (b) are 1V, 100pA and -50mV, 200 pA, respectively. The sample bias for all the AP-STM images is -0.2 V.

Monolayer iron oxide was prepared by depositing iron on Au(111) in 10^{-7} mbar O_2, followed by cooling the sample in 10^{-7} mbar O_2 to RT. The coverage can be precisely controlled by tuning the deposition time. Fig. 1(a) is a large scale STM image of 0.8 monolayers (ML) FeO on Au(111), whereby 1ML corresponds to a fully covered FeO film on Au(111). The FeO island exhibits a height of 1.5 Å along with a modulated Moiré pattern of 3.2 nm due to the lattice mismatch. The triangular loops are O adatom dislocation lines where the Fe atoms are four-fold coordinated[58]. As a result, these lines appear bright in STM topography[22,59], as shown in the enlarged STM image of Fig. 1(b). In addition to FeO(111), other metal oxide thin films on well-defined metal substrates also exhibit such feature, such as CoO bilayer on Au(111)[60] and Pt(111)[61], which depends on the oxygen pressure. In our control experiments, the iron oxide prepared without cooling in oxygen exhibits no such lines (Fig. S1 in supporting information). As the CUF sites are active for O_2 dissociation, we prepared FeO islands at low coverage on which the density of O adatom dislocation lines is much higher than that in the large island, as shown in Fig. 1(c). Fig. 1(d) is an enlarged STM image taken from the white square in panel (c) that presents the dislocation lines with matched orientation with respect to the high-symmetric direction on the Au(111) substrate. The island marked by "i" was used as a reference to show the sequential scan in the same area (because of the drift during scan in our AP-STM system). The corresponding line profile selected to cross the pristine FeO island presents a thickness of ~1.5 Å, while the dislocation lines have a height of ~0.8 Å (Fig. S2). Introducing 1.5 mbar CO into the reactor cell, neither the FeO islands nor the Au substrate shows any morphology change (dislocation lines), even after extending the exposure time (Fig. 1(e) and 1(f)). This finding is consistent with previous experimental results that bare FeO is inert to CO oxidation[37] under the conditions used in temperature-programmed desorption/reaction (TPD, TPR) studies[42, 62]. The observed dislocation lines are indicated with the ball sketch in Fig. 1(g). These dislocation lines have been reported previously in the case of lattice displacements due to the formation of four-coordinated metal atoms within metal oxide films supported on Au(111)[58] and Pt(111)[63]. Schematic models in Fig. 1(h) depict the 4-fold coordinated Fe atom along the dislocation lines

and the perfect FeO island with the 3-fold coordinated Fe atoms.

After CO exposure, the reactor cell was evacuated to UHV (10^{-8} mbar), followed by introducing 10^{-2} mbar O_2. Fig. 2(a) shows the same scanning area before introducing O_2 gas. The dislocation lines on FeO disappear simultaneously after O_2 exposure. These islands are referred as FeO_x to distinguish them from the freshly prepared films. Meanwhile, the FeO_x islands and Au surface are decorated with bright dots (Fig. 2(b)). These images were recorded under 10^{-2} mbar O_2 at 300 K. Fig. 2(c) to 2(e) are sequential scans taken after O_2 exposure for 3 mins, 8 mins and 14 mins, respectively. The white and yellow arrows highlight adsorbates on FeO islands and Au(111) with an average size of ~0.8 nm (Fig. S3, supporting information), respectively. These species are highly mobile at the initial stage of O_2 exposure. After 20 mins, the whole surface was in an equilibrium situation without further change on morphology, as shown in Fig. 2(f). Compared to the bilayer FeO before O_2 exposure, the FeO_x islands are still atomically flat but with an increased height of 4.0Å, suggesting the incorporation of a layer of O atoms[37]. Fig. 2(f)

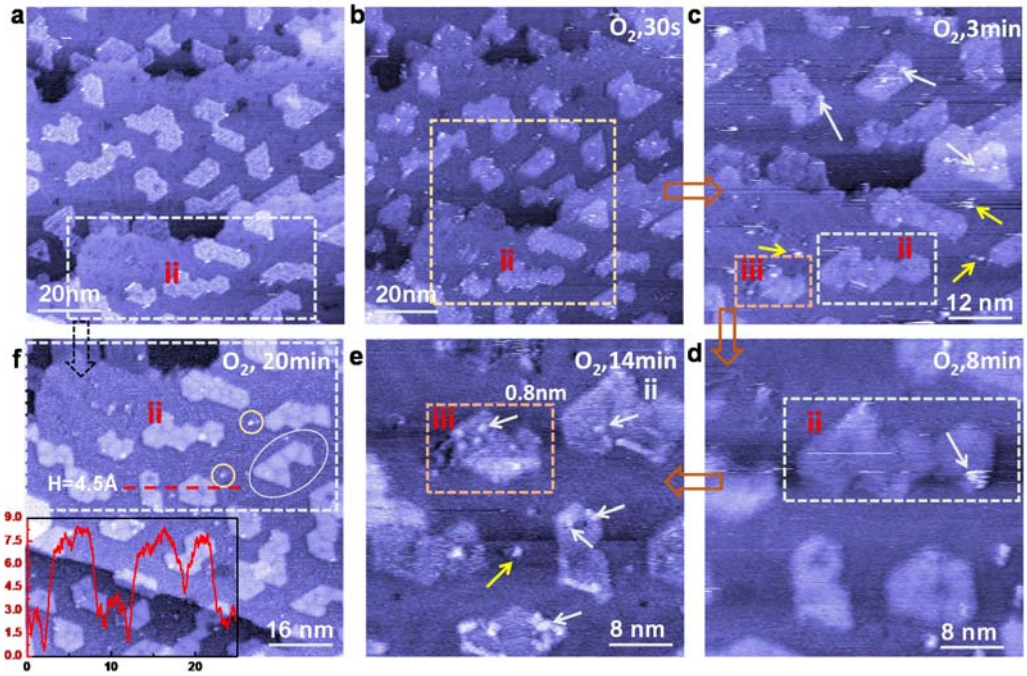

FIG. 2. Disappearance of dislocation lines after O_2 exposure. (a) Large-scale STM image of FeO/Au(111) after the evacuation of CO; (b) the same area after introducing 10^{-2} mbar O_2; island marked with "ii" is used as a reference to show the morphology change; (c) after 3mins, all the dislocation lines disappeared; the white and yellow

arrows indicate the mobile clusters on FeO_x islands and Au surface, respectively; (d) Zoom in scan shows the disappearance of dislocation lines on "ii"; (e) Exposure to 10^{-2} mbar O_2 for 14 mins. White and yellow arrows indicate the bright spots on FeO_x islands and Au surface, respectively; (f) The FeO_x islands get equilibrium after exposure for 20min under 10^{-2} mbar O_2. The line-scan profile is taken along the red-dashed line in (f). The sample bias for all the images is -0.1 V.

shows the transformation of the dislocation lines into dark-colored lines on each island after O_2 exposure. The whole processes demonstrate the oxygen activation along both the edges of FeO islands and the lines, which have also been detected on cobalt oxide islands comprising dislocation lines[64]. The morphology of FeO_x islands remained unchanged in UHV after the evacuation of O_2 (Fig. 3(a)), which is crucial for *ex situ* XPS measurements.

B. Reduction of FeO_x(111) islands in CO

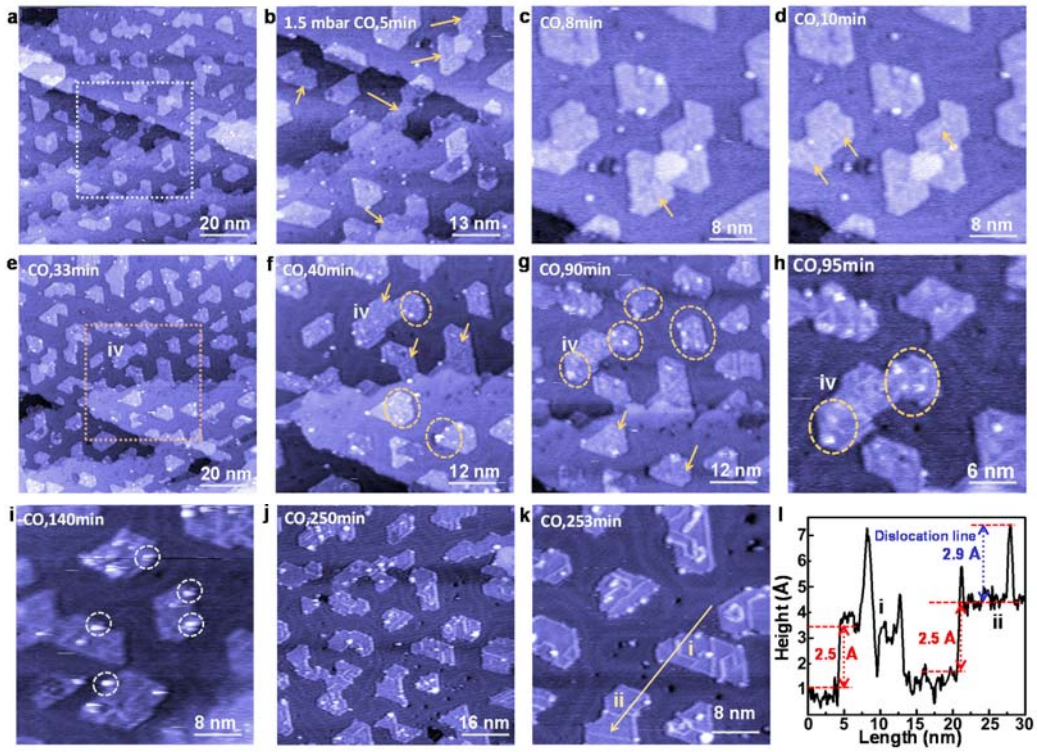

FIG. 3. Regeneration of dislocation lines after CO exposure. (a). large-scale STM image of FeO_x/Au(111) after the evacuation of O_2; (b). Image taken from the square in a after introducing 1.5 mbar CO. The yellow arrows highlight the reappearance of dislocation lines on FeO_x islands; (c). Zoom-in scan from the up-right of panel b showing the reappearance of dislocation lines (yellow arrows); (d). sequential scan after CO exposure for 10min, the yellow arrows show more dislocations lines than those in c; (e-h): island "iv" is used as a reference to show the generation of mobile bright spots (dashed ellipsoids in f-h); (i-k): After CO exposure for more than 2 hrs. AP-STM image

shows the stabilization of the bright spots and the regeneration of dislocation lines; (l) Line-scan profile taken along the yellow arrow in (k). The CO exposure time is imposed at the up-left corner of each panel.

In the next stage, we exposed the iron oxide islands to 1.5 mbar CO at RT by monitoring the morphology changes. The FeO_x islands after CO exposure are denoted by R-FeO_x. Since there are excess O adatoms on the FeO_x islands, oxidation of CO is expected[37]. Fig. 3(a) is a large-scale STM image of the FeO_x islands after evacuation of O_2. Fig. 3(b)-(d) are sequential scanning images under 1.5 mbar CO. The yellow arrows highlight the regeneration of dislocation lines after CO exposure [Fig. 3(d)]. The smaller the island is, the longer time required to regenerate the dislocation lines, which can be ascribed to size-dependent structural dynamics[65], as can be seen in Fig. 3(d) after CO exposure for 10 mins. Meanwhile, highly mobile bright-spots reappear on R-FeO_x islands and Au(111), as highlighted by dashed ellipsoids in Figs. 3(e)-(g). A zoom-in scan of Fig. 3(h) clearly shows the regeneration of dislocation lines (arrows), while the bright dots still can be detected even after CO exposure for more than 100 mins (circles in Fig. 3(i)).

Further increasing the CO exposure time, neither morphology change on the R-FeO_x islands nor the mobile spot has been observed after reaching equilibrium (Fig. 3(j)). The dislocation lines are clearly visible, while the bright spots are still stabilized on each island, as shown in the zoom-in scan of Fig. 3(k). Furthermore, compared with the thickness of pristine and oxidized FeO_x islands, CO exposure leads to an average height of ~2.5Å, indicating the removal of O atoms, as plotted in Fig. 3(l) (Fig. S4, supporting information). It is noted that all the images used for line profile measurements were taken under UHV at RT after evacuating the reactor cell with sample bias of -0.1 and -0.2 V to minimize the effect of local density of electronic states.

C. XPS studies of the oxidation and reduction processes

Surface species after AP-STM imaging after each reaction step were interrogated by XPS measurements. As shown in Fig. 4(a), the Fe 2*p* core levels are split into $2p_{1/2}$ and $2p_{3/2}$ components due to the spin-orbit coupling. The Fe $2p_{3/2}$ core level spectra for elemental Fe on Au(111) and FeO(111)/Au(111) is located at 706.9 eV and 709.62 eV,

respectively, which agrees with the literature values[42]. The asymmetrically broadened Fe $2p_{3/2}$ peak of FeO is due to a satellite excitation of the Fe^{2+} species[66]. The Fe 2*p* peak shifted to 709.07 eV after exposing to 1.5 mbar CO for 1 hr. Since there is no morphological change on the dislocation lines, the lattice oxygen at the oxide/metal interface may be involved directly in the CO oxidation[67], leading to partial reduction of FeO at the edges. The Fe 2*p* peak shifted to 710.41 eV after 10^{-2} mbar O_2 exposure.

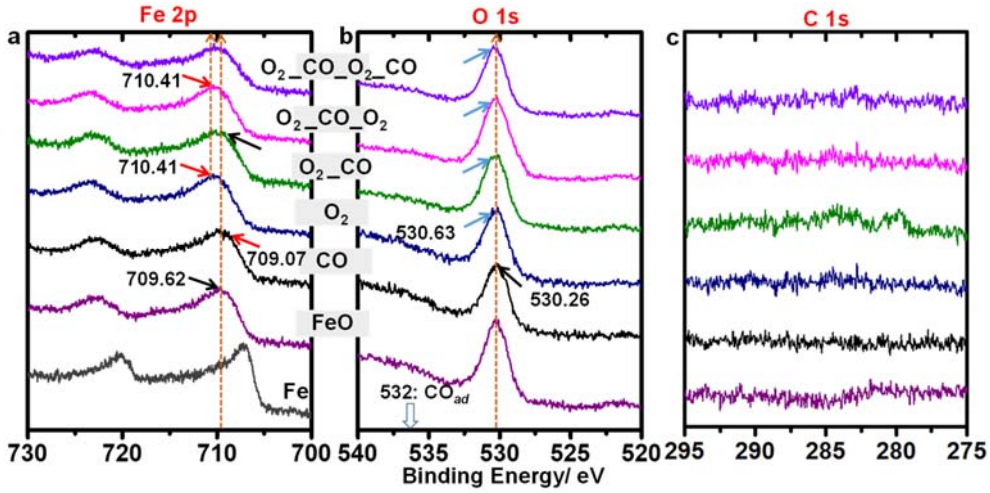

FIG. 4. (a) Fe 2*p*, (b) O 1*s* and (C) C 1*s* XPS spectra acquired of (from bottom to top): fresh iron island on Au(111) (only in a); fresh FeO/Au(111); after CO exposure only; after O_2 exposure only; first O_2 exposure, then evacuate the reactor cell, and finally CO exposure; alternate O_2, CO and O_2 exposure; and two cycles of O_2 and CO exposure, as the reaction conditions shown. The O_2 and CO pressure used in each cycle is controlled in the range of $1\sim2\times10^{-2}$ mbar and 1.5~1.9 mbar, respectively.

One probable reason is the formation of trilayer O-Fe-O because the binding energy is comparable with FeO_2 islands on Pt(111) that the peak position of Fe $2p_{3/2}$ shifts to 710.1 eV after O_2 exposure[29]. However, the peak intensity exhibits a minor increase, which is significantly different from the doubling peak intensity of FeO_2 on Pt(111). Furthermore, according to previous XPS studies on the O-M-O trilayer, the oxygen atoms at the upper- and lower-side exhibit a lower and higher binding energy, respectively[29]. The transformation of FeO to FeO_2 is therefore probably due to the intercalation of O atoms at the interface between FeO and the metal substrate. Accordingly, the O 1*s* should have a new peak at higher binding energy[29]. A new peak detected at 530.63 eV is higher than that of pristine FeO, and it is assigned to O atoms

incorporated on FeO terraces [Fig. 4(b)]. This assignment is consistent with the AP-STM images where the dislocation lines disappeared along with increase in the height of FeO islands. It is noteworthy from the XPS results that the peak shape and position of Fe $2p_{3/2}$ have minimal change in each cycle after CO exposure (see details in methods). As the iron oxide islands are stable after evacuating the reactor cell, we proceeded to repeat reaction cycles by sequential O_2 and CO exposure. O_2 exposure leads to increased intensity of the peak at 710.4 eV, whereas CO exposure has no significant impact on the peaks. The binding energy of the O 1*s* peak is independent of the oxide phase[29,68], the main peak after different reactions still located at 530.26 eV, as shown in Fig. 4(b).

In contrast to the reduction of FeO/Au(111) in CO at elevated temperature and pressures which is deactivated by significant formation of carbonates and FeC_x, FeO islands can be regenerated after CO exposure at 300 K and moderate pressures, where no FeC_x (indicated by a characteristic feature at 708.5eV)[41,69] is detected by XPS. As shown in Fig. 4(c), C 1*s* spectrum point to the absence of carbonates as well (290 eV for CO_3)[41]. As the accumulation of carbon species can severely deactivate iron oxide catalysts, it is essential to either suppress the formation of carbon-containing species or remove these adsorbates effectively during reactions[70]. As the reaction temperature and pressure of reactant significantly influence the surface reactions, precise control of pressures (1.5~1.9 mbar CO) and sequential exposure to reactants would be a probable way to avoid the formation of carbon-containing species.

D. High activity of O-activated FeO for CO oxidation: DFT studies

To correlate the reversible oxidation and reduction of FeO(111) supported on Au(111) with the mechanism of CO oxidation, we performed DFT calculations. The surface structure of FeO(111) is depicted in Fig. 5a, with the oxygen atoms exposed to the vacuum[41]. We optimized the adsorption configurations of CO, O and CO_2 on

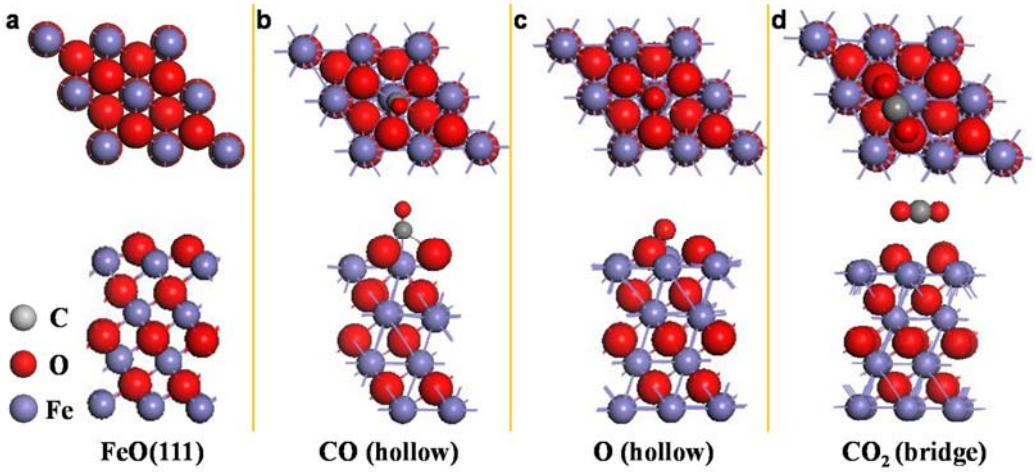

FIG. 5. Top and side views of (a) optimized FeO(111) surface; adsorption configurations of (b) CO, (c) O and (d) CO_2 on the FeO(111) surface. Carbon, oxygen and iron atoms were represented as gray, red and blue balls.

Table 1 The adsorption sites, adsorption energies and key parameters for related species on FeO(111) surface.

Surface	Species	Configurations	Bond lengths/Å	Adsorption energies/eV
FeO(111)	CO	fcc, C-bound	$d_{C\text{-}O}$ = 1.19	-1.39
	O	fcc, O-bound	$d_{O\text{-}O}$ = 2.42	-2.58
	CO_2	top, away from the surface	N. A.	-0.07

the FeO(111) surface, and calculated the adsorption energies at different active sites (Table 1). Fig. 5(b)-(d) demonstrated the most stable configurations of CO, O and CO_2 on FeO(111), respectively. Both the CO and O atoms prefer to reside at the face-centered cubic (fcc) hollow sites. The calculated adsorption energy of CO is -1.39 eV, in accordance with previous reports (-1.41 eV)[71]. Individual O atoms have a much higher adsorption energy. In the case of CO_2, results indicate its weak physisorbtion on the FeO(111) surface with a negligible value of -0.07 eV, suggesting that it can easily desorb from the surface (Fig. 5d). Meanwhile, the pre-adsorption of oxygen on FeO(111) weakened CO adsorption to -1.16 eV. The decrease in energy has a profound impact on the kinetics of CO oxidation. To examine the catalytic activity toward CO oxidation on

different surfaces, we explored the MvK mechanism for the oxidation of CO on bare and O pre-covered FeO(111) surface.

Two different reaction pathways were explored by using the adsorption configuration of CO_2 as the final state. Fig. 6 demonstrated the calculated potential energy surface for the CO oxidation reaction on different surfaces. Initial states (IS), transition states (TS) and final states (FS) of two different reaction pathways are depicted in each stage. Starting from the bare FeO(111) surface which followed the MvK mechanism, as shown in Fig. 6 (top row). The adsorbed CO molecule at the fcc hollow site can easily diffuse to the bridge site (TS1). CO reacts with the nearby lattice oxygen when it is adsorbed on the bridge side (green arrow in TS1), forming chemisorbed CO_2. Finally, the CO_2 weakly physisorbed above the surface

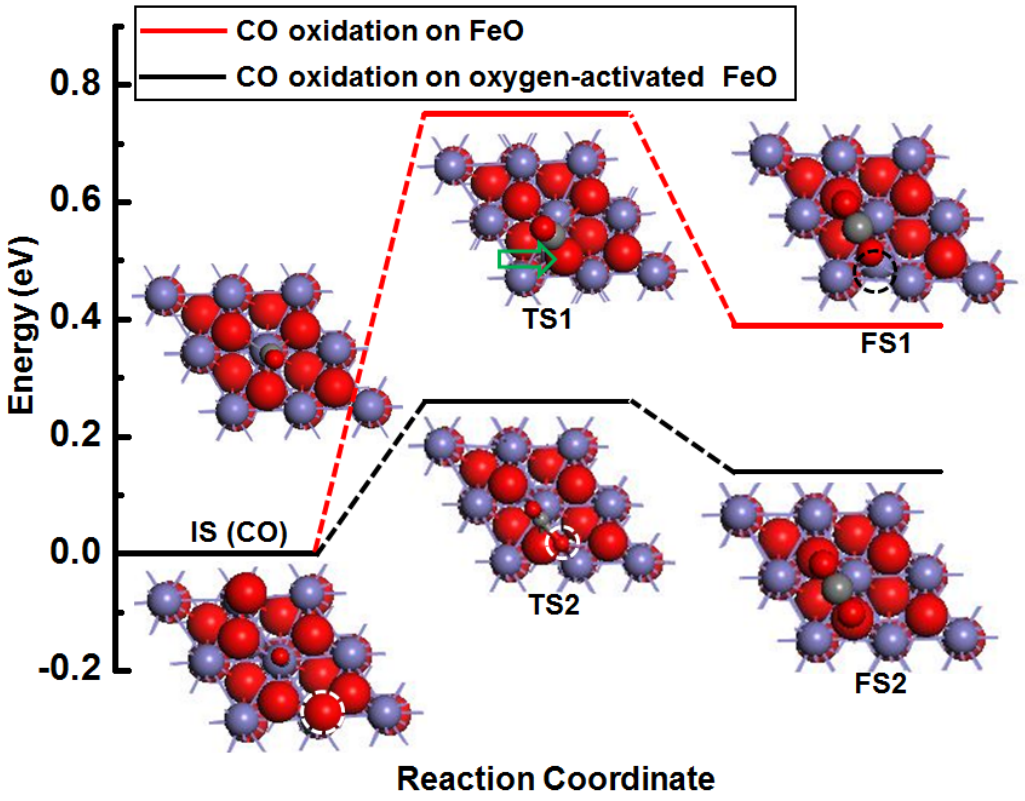

FIG. 6. Potential energy profiles of CO oxidation on FeO(111) surfaces. Theoretical models are corresponding to the initial states (IS), transition state (TS) and final state (FS) in two different reaction pathways are imposed. The green arrow in TS1 indicates the lattice oxygen in FeO island; the dashed-black circle represents the missing lattice oxygen that participates the surface reaction to form CO_2; dashed-white circles in the

bottom reaction path indicate the adsorbed O atom on FeO. Carbon, oxygen and iron atoms are represented as gray, red and blue balls.

Table 2 Energies of CO oxidation reaction on different FeO(111) surfaces

Surfaces	Reactions	TS	$E(b)_f$/eV	ΔH/eV
FeO(111)	$CO + O_{lattice} \rightarrow CO_2$	TS1	0.75	0.39
O-FeO(111)	$CO + O_{ads} \rightarrow CO_2$	TS2	0.26	0.14

$E(b)_f$ is the energy barrier of the forward reaction; ΔH is the reaction energy.

(FS1). The reaction is endothermic (0.39 eV), with an energy barrier of 0.75 eV (Table 2). The rate-determining step is extracting lattice oxygen, which is a common barrier for many surface reactions involving lattice oxygen[72,73].

Next, we examined the CO oxidation reaction on an O-decorated FeO(111) surface. In our study, to reduce the computational complexity, we modeled the oxygen pre-covered surface by using an individual O atom[44]. The O_2 dissociation is the rate-determining step in CO oxidation on types of catalysts[74]. Formation of strong C-O bond in CO_2 overcompensates the energy cost of removing the O atom from the surface. As demonstrated previously, the formation energy of an oxygen vacancy on FeO_2/Pt(111) (1.3 eV) is about half of that on the pristine FeO/Pt(111) (2.8 eV)[70]. In current case, the dislocation lines activated O_2 on the FeO terrace and incorporated O atoms that would reduce the reaction barrier. As depicted in the bottom row of Fig. 6, a CO molecule diffused from the fcc hollow site to the bridge site, which located closer to the adsorbed O atom (TS2, highlighted by the circle). Subsequently, the CO molecule reacted with the O atom, forming chemisorbed CO_2. The reaction barrier for this process was calculated to be 0.26 eV with an endothermic value of 0.14 eV (Table 2). Clearly, the FeO surface with pre-adsorbed O atoms is more reactive than bare surface. Note that, in our model, only the reaction at the flat terraces of the FeO film was considered. The CO interaction at the edges of FeO islands even without oxygen pretreatment, revealed by XPS, can occur at a lower energy cost[75].

IV. CONCLUSIONS

In summary, we performed AP-STM and XPS to study the oxidation and reduction of FeO(111) islands supported on Au(111) surface. The disappearance of dislocation lines upon O_2 oxidation resulted in the incorporation of excess O atoms on the oxide islands. Exposing CO gas caused the regeneration of dislocation lines that correlated with the promotion of CO oxidation by surface O atoms. DFT calculations compared the reaction barriers of CO on bare and oxygen modified FeO(111) surfaces, revealing a significant energy barrier drop after introducing adsorbed oxygen atoms. Excess oxygen on metal oxide surfaces could therefore be used to activate or regenerate actives sites for oxidation nanocatalysts.

SUPPLEMENTARY MATERIAL

See the supplementary material for STM images of FeO/Au(111).

Notes

The authors declare no competing financial interest.

ACKNOWLEDGMENTS:

Authors acknowledge the financial support from Natural Science Foundation of Jiangsu Province BK20181297. DJS was supported by Integrated Mesoscale Architectures for Sustainable Catalysis (IMASC), an Energy Frontier Research Center funded by the U.S. Department of Energy, Office of Science, Basic Energy Sciences under Award #DE SC0012573. This research used resources of the Center for Functional Nanomaterials, which is a U.S. DOE Office of Science Facility, at Brookhaven National Laboratory under Contract No. DE-SC0012704.

REFERENCES

[1] A. Picone, M. Riva, A. Brambilla, A. Calloni, G. Bussetti, M. Finazzi, F. Ciccacci, and L. Duò, "Reactive Metal-oxide Interfaces: A Microscopic View," *Surf. Sci. Rep.* **71**, 32-76(2016).

[2] Q. Fu, and T. Wagner, "Interaction of Nanostructured Metal Overlayers With Oxide Surfaces," *Surf. Sci. Rep.* **62**, 431-498(2017).

[3] A. Zavabeti, J. Z. Ou, B. J. Carey, N. Syed, R. Orrell-Trigg, E. L. H. Mayes, C. Xu, O. Kavehei, A. P. O'Mullane, R. B. Kaner, K. Kalantar-zadeh, and T. Daeneke, "A Liquid Metal Reaction Environment for the Room-temperature Synthesis of Atomically Thin Metal Oxides," *Science* **358**, 332-335(2017).

[4] J. A. Rodriguez, P. Liu, J. Graciani, S. D. Senanayake, D. C. Grinter, D. Stacchiola, J. Hrbek, and J. Fernández-Sanz, "Inverse Oxide/Metal Catalysts in Fundamental Studies and Practical Applications: A Perspective of Recent Developments," *J. Phys. Chem. Lett.* **7**, 2627-2639(2016).

[5] J. Zhang, H. Wang, L. Wang, S. Ali, C. Wang, L. Wang, X. Meng, B. Li, D. Su, and F. Xiao, "Wet-

Chemistry Strong Metal–Support Interactions in Titania-Supported Au Catalysts," *J. Am. Chem. Soc.* **141**, 2975-2983(2019).
[6] G. S. Parkinson, "Iron Oxide Surfaces," *Surf. Sci. Rep.* **71**, 272-365(2016).
[7] I. Ro, I. B. Aragao, J. P. Chada, Y. Liu, K. R. Rivera-Dones, M. R. Ball, D. Zanchet, J. A. Dumesic, and G. W. Huber, "The Role of Pt-Fe_xO_y Interfacial Sites for CO Oxidation," *J. Catal.* **358**, 19-26(2018).
[8] M. D. Santis, A. Buchsbaum, P. Varga, and M. Schmid, "Growth of Ultrathin Cobalt Oxide Films on Pt(111)," *Phys. Rev. B* **84**, 125430(2011).
[9] J. Fester, M. García-Melchor, A. S. Walton, M. Bajdich, Z. Li, L. Lammich, A. Vojvodic, and J. V. Lauritsen, "Edge Reactivity and Water-assisted Dissociation on Cobalt Oxide Nanoislands," *Nat. Commun*. **8**, 14169(2017).
[10] I. Szenti, L. Bugyi, and Z. Kónya, "The Promotion of CO Dissociation by Molybdenum Oxide Overlayers on Rhodium," *Surf. Sci.* **657**, 1-9(2017).
[11] X. Zhou, G. J. A. Mannie, J. Yin, X. Yu, C. J. Weststrate, X. Wen, K. Wu, Y. Yang, Y. Li, and J. W. Niemantsverdriet, "Iron Carbidization on Thin-Film Silica and Silicon: A Near-Ambient-Pressure X-ray Photoelectron Spectroscopy and Scanning Tunneling Microscopy Study," *ACS Catal*. **8**, 7326-7333(2018).
[12] C. Xu, G. Chen, Y. Zhao, P. Liu, X. Duan, L. Gu, G. Fu, Y. Yuan, and N. Zheng, "Interfacing with Silica Boosts the Catalysis of Copper," *Nat. Commu.* **9**, 3367(2018).
[13] J. Graciani, K. Mudiyanselage, F. Xu, A. E. Baber, J. Evans, S. D. Senanayake, D. J. Stacchiola, P. Liu, J. Hrbek, J. F. Sanz1, and J. A. Rodriguez, "Highly Active Copper-ceria and Copper-ceria-titania Catalysts for Methanol Synthesis from CO_2," *Science* **345**, 546-550(2014).
[14] J. IngoFlege, and D. C. Grinter, "*In situ* Studies of Oxide Nucleation, Growth, and Transformation Using Slow Electrons," *Prog. Surf. Sci.* **93**, 21-45(2018).
[15] C. Ratnasamy, J. P. Wagner, Water Gas Shift Catalysis. *Catal. Rev.* **51**, 325-440(2009).
[16] M. Zhu, T. C. R. Rocha, T. Lunkenbein, A. Knop-Gericke, R. Schlögl, and I. E. Wachs, "Promotion Mechanisms of Iron Oxide-Based High Temperature Water-Gas Shift Catalysts by Chromium and Copper," *ACS Catal.* **6**, 4455–4464(2016).
[17] I. Ro, I. B. Aragao, J. P. Chada, Y. Liu, K. R. Rivera-Dones, M. R.Ball, D. Zanchet, J. A. Dumesic, and G. W. Huber, "The Role of Pt-Fe_xO_y Interfacial Sites for CO Oxidation," *J. Catal.* **358**, 19-26 (2018).
[18] H. Chen, Y. Liu, F. Yang, M. Wei, X. Zhao, Y. Ning, Q. Liu, Y. Zhang, Q. Fu, and X. Bao, "Active Phase of FeO_x/Pt Catalysts in Low-Temperature CO Oxidation and Preferential Oxidation of CO Reaction," *J. Phys. Chem. C* **121**, 10398-10405(2017).
[19] H. J. Freund, "Oxygen Activation on Oxide Surfaces: A Perspective at the Atomic Level," *Catal. Today* **238**, 2-9(2014).
[20] I. N. Remediakis, N. Lopez, and J. K. Nørskov, "CO Oxidation on Rutile-Supported Au Nanoparticle," *Angew. Chem. Int. Ed.* **44**, 1824–1826(2005).
[21] R. A. Ojifinni, N. S. Froemming, J. Gong, M. Pan, T. S. Kim, J. M. White, G. Henkelman, and C. Buddie Mullins, "Water-Enhanced Low-Temperature CO Oxidation and Isotope Effects on Atomic Oxygen-Covered Au(111)," *J. Am. Chem. Soc.* **130**, 6801-6812(2008).
[22] Q. Pan, X. Weng, M. Chen, L. Giordano, G. Pacchioni, C. Noguera, J. Goniakowski, S. Shaikhutdinov, and H. J. Freund, "Enhanced CO Oxidation on the Oxide/Metal Interface: From Ultra-High Vacuum to Near-Atmospheric Pressures," *Chem. Cat Chem.* **7**, 2620-2627(2015).
[23] R. Toyoshima, M. Yoshida, Y. Monya, K. Suzuki, K. Amemiya, K. Mase, B. S. Mun, and H. Kondoh, "*In Situ* Photoemission Observation of Catalytic CO OxidationReaction on Pd(110) under Near-Ambient Pressure Conditions: Evidence for the Langmuir−Hinshelwood Mechanism," *J. Phys. Chem. C* **117**, 20617-20624(2013).
[24] D. Widmann, and R. J. Behm, "Activation of Molecular Oxygen and the Nature of the Active Oxygen Species for CO Oxidation on Oxide Supported Au Catalysts," *Acc. Chem. Res.* **47**, 740-749(2014).
[25] D. Widmann, and R. J. Behm, "Dynamic Surface Composition in a Mars-van Krevelen Type Reaction: CO Oxidation on Au/TiO_2," *J. Catal.* **357**, 263-273(2018).
[26] Q. Fu, W. Li, Y. Yao, H. Liu, H. Su, D. Ma, X. Gu, L. Chen, Z. Wang, H. Zhang, B. Wang, and X. Bao, "Interface-Confined Ferrous Centers for Catalytic Oxidation," *Science* **328**, 1141-1144(2010).
[27] H. Zeuthen, W. Kudernatsch, L. R. Merte, L. K. Ono, L. Lammich, F. Besenbacher, and S. Wendt, "Unraveling the Edge Structures of Platinum(111)-supported Ultrathin FeO Islands: The Influence of Oxidation State," *ACS Nano* **9**, 573-583(2015).
[28] W. Kudernatsch, G. Peng, H. Zeuthen, Y. Bai, L. R. Merte, L. Lammich, F. Besenbacher, M. Mavrikakis, and S. Wendt, "Direct Visualization of Catalytically Active Sites at the FeO-Pt(111) Interface," *ACS Nano* **9**, 7804-7814(2015).
[29] Q. Fu, Y. Yao, X. Guo, M. Wei, Y. Ning, H. Liu, F. Yang, Z. Liu, and X. Bao, "Reversible Structural

Transformation of FeO_x Nanostructures on Pt Under Cycling Redox Conditions and Its Effect on Oxidation Catalysis," *Phys. Chem. Chem. Phys.* **15**, 14708-14714(2013).
[30] L. M. Molina, M. D. Rasmussen, and B. Hammer, "Adsorption of O_2 and Oxidation of CO at Au Nanoparticles Supported by TiO_2(110)," *J. Chem. Phys.* **120**, 7673–7680(2004).
[31] A. R. Puigdollers, P. Schlexer, S. Tosoni, and G. Pacchioni, "Increasing Oxide Reducibility: The Role of Metal/Oxide Interfaces in the Formation of Oxygen Vacancies," *ACS Catal.* **7**, 6493-6513(2017).
[32] F. Esch, S. Fabris, L. Zhou, T. Montini, C. Africh, P. Fornasiero, G. Comelli, and R. Rosei, "Electron Localization Determines Defect Formation on Ceria Substrates," *Science* **309**, 752(2005).
[33] Y. Jin, G. Sun, F. Xiong, L. Ding, and W. Huang, "Water-Activated Lattice Oxygen in FeO(111) Islands for Low Temperature Oxidation of CO at Pt−FeO Interface," *J. Phys. Chem. C* **120**, 9845−9851(2016).
[34] J. Saavedra, H. A. Doan, C. J. Pursell, L. C. Grabow, and B. D. Chandler, "The Critical Role of Water at the Gold-Titania Interface in Catalytic CO Oxidation," *Science* **345**, 1599(2014).
[35] M. A. van Spronsen, K. J. Weststrate, and L. B. F. Juurlink, "A Comparison of CO Oxidation by Hydroxyl and Atomic Oxygen from Water on Low-Coordinated Au Atoms," *ACS Catal.* **6**, 7051-7058(2016).
[36] H. Jeong, J. Bae, J. W. Han, and H. Lee, "Promoting Effects of Hydrothermal Treatment on the Activity and Durability of Pd/CeO_2 Catalysts for CO Oxidation," *ACS Catal.* **7**, 7097-7105(2017).
[37] Y. Sun, L. Giordano, J. Goniakowski, M. Lewandowski, Z. Qin, C. Noguera, S. Shaikhutdinov, G. Pacchioni, and H. J. Freund, "The Interplay between Structure and CO Oxidation Catalysis on Metal Supported Ultrathin Oxide Films," *Angew. Chem.* **122**, 4520-452(2010).
[38] K. Zhang, L. Li, S. Shaikhutdinov, and H. J. Freund, "Carbon Monoxide Oxidation on Metal-Supported Monolayer Oxide Films: Establishing Which Interface is Active," *Angew. Chem. Int. Ed.* **57**, 1261-1265(2018).
[39] J. Saavedra, C. Powell, B. Panthi, C. J. Pursell, and B. D.Chandler, "CO Oxidation over Au/TiO_2 Catalyst: Pretreatment Effects, Catalyst Deactivation, and Carbonates Production," *J. Catal.* **307**, 37-47(2013).
[40] Y. Denkwitz, Z. Zhao, U. Hörmann, U. Kaiser, V. Plzak, and R. J. Behm, "Stability and Deactivation of Unconditioned Au/TiO_2 Catalysts During CO Oxidation in a Near-Stoichiometric and O_2-Rich Reaction atmosphere," *J. Catal.* **251**, 363-373(2007).
[41] L. Yu, Y. Liu, F. Yang, J. Evans, J. A. Rodriguez, and P. Liu, "CO Oxidation on Gold-Supported Iron Oxides: New Insights into Strong Oxide-Metal Interactions," *J. Phys. Chem. C* **119**, 16614-16622(2015).
[42] Weiss, W.; Ranke, W. Surface Chemistry and Catalysis on Well-defined Epitaxial Iron-Oxide Layers. *Prog. Surf. Sci.* **70,** 1-151 (2002).
[43] B. Qiao, A. Wang, X. Yang, L. Allard, Z. Jiang, Y. Cui, J. Liu, J. Li, and T. Zhang, "Single-Atom Catalysis of CO Oxidation Using Pt_1/FeO_x," *Nat. Chem.* **3**, 634–641(2011).
[44] Y. Wang, D. C. Cantu, M. Lee, J. Li,V. A. Glezakou, and R. Rousseau, "CO Oxidation on Au/TiO_2: Condition-dependent Active Sites and Mechanistic Pathway," *J. Am. Chem. Soc.* **138**, 10467-10476(2016).
[45] F. Tao, S. Dag, L. Wang, Z. Liu, D. R. Butcher, H. Bluhm, M. Salmeron, and G. A.Somorjai, "Break-Up of Stepped Platinum Catalyst Surfaces by High CO Coverage," *Science* **327**, 850-853(2010).
[46] F. Tao, W. T. Ralston, H. Liu, and G. A.Somorjai, "Surface Structures of Model Metal Catalysts in Reactant Gases," *J. Phys. Chem. B* **122**, 425-431(2018).
[47] M. A. van Spronsen, J. W. M. Frenken, and I. M. N. Groot, "Observing the Oxidation of Platinum," *Nat. Commnun.* **8**, 429(2017).
[48] F. Tao, D. Tang, M. Salmeron, and G. A. Somorjai, "A New Scanning Tunneling Microscope Reactor Used for High-pressure and High-temperature Catalysis Studies," *Rev. Sci. Instrum.* **79**, 084101(2008).
[49] F. Besenbacher, P. Thostrup, and M. Salmeron, "The Structure and Reactivity of Surfaces Revealed by Scanning Tunneling Microscopy," *MRS Bull.* **37**, 677-681(2012).
[50] M. Salmeron, and R. Schlögl, "Ambient Pressure Photoelectron Spectroscopy: A New Tool for Surface Science and Nanotechnology," *Surf. Sci. Rep.* **63**, 169-199(2008).
[51] J. Kim, M. C. Noh, W. H. Doh, and J, Y. Park, "*In Situ* Observation of Competitive CO and O_2 Adsorption on the Pt(111) Surface Using Near-Ambient Pressure Scanning Tunneling Microscopy," *J. Phys. Chem. C* **122**, 6246-6254(2018).
[52] V. Navarro, M. A. van Spronsen, and J. W. M. Frenken, "*In situ* Observation of Self-assembled Hydrocarbon Fischer−Tropsch Products on a Cobalt Catalyst," *Nat. Chem.* **8**, 929−934(2016).
[53] T. Niu, Z. Jiang, Y. Zhu, G. Zhou, M. A. van Spronsen, S. A. Tenney, J. Anibal Boscoboinik, and D. Stacchiola, "Oxygen-Promoted Methane Activation on Copper," *J. Phys. Chem. B* **122**, 855-863(2018).
[54] M. C. Payne, M. P. Teter, D. C. Allan, T. A. Arias, and J. D. Joannopoulos, "Iterative Minimization Techniques for Abinitio Total-Energy Calculations - Molecular-Dynamics and Conjugate Gradients," *Rev.*

Mod. Phys. **64**, 1045-1097 (1992).
[55] J. P. Perdew, K. Burke, and Y. Wang, "Generalized Gradient Approximation for the Exchange-Correlation Hole of a Many-Electron System," *Phys. Rev. B* **54**, 16533 (1996).
[56] H. J. Kulik, N. Marzari, "Transition-Metal Dioxides: A Case for the Intersite Term in Hubbard-Model Functionals," *J. Chem. Phys.* **134**, 094103 (2011).
[57] T. A. Halgren, and W. N. Lipscomb, "Synchronous-Transit Method for Determining Reaction Pathways and Locating Molecular Transition-States," *Chem. Phys. Lett.* **49**, 225-232 (1977).
[58] Y. Li, K. C. Adamsen, L. Lammich, J. V. Lauritsen, and S. Wendt, "Atomic-Scale View of the Oxidation and Reduction of Supported Ultrathin FeO Islands," *ACS Nano* **13**, 11632-11641 (2019).
[59] L. R. Merte, Y. Bai, H. Zeuthen, G. Peng, L. Lammich, F. Besenbacher, M. Mavrikakis, and S. Wendt, "Identification of O-rich Structures on Platinum (111)-Supported Ultrathin Iron Oxide Films," *Surf. Sci.* **652**, 261-268(2016).
[60] A. S. Walton, J. Fester, M. Bajdich, M. A. Arman, J. Osiecki, J. Knudsen, A. Vojvodic, and J. V. Lauritsen, "Interface Controlled Oxidation States in Layered Cobalt Oxide Nanoislands on Gold," *ACS Nano* **9**, 2445-2453(2015).
[61] J. Fester, Z. Sun, J. Rodríguez-Fernandez, A. Walton, and J. V. Lauritsen, "Phase Transitions of Cobalt Oxide Bilayers on Au(111) and Pt(111): The Role of Edge Sites and Substrate Interactions," *J. Phys. Chem. B* **122**, 561-571(2018).
[62] Y. Sun, Z. Qin, M. Lewandowski, E. Carrasco, M. Sterrer, S. Shaikhutdinov, and H. J. Freund, "Monolayer Iron Oxide Film on Platinum Promotes Low Temperature CO Oxidation," *J. Catal.* **266**, 359-368(2009).
[63] X. Deng, and H. Tüysüz, "Cobalt-Oxide-Based Materials as Water Oxidation Catalyst: Recent Progress and Challenges," *ACS Catal.* **4**, 3701−3714(2014).
[64] J. Fester, M. Bajdich, A. S. Walton, Z. SunPhilipp, N. Plessow, A. Vojvodic, and J. V. Lauritsen, "Comparative Analysis of Cobalt Oxide Nanoisland Stability and Edge Structures on Three Related Noble Metal Surfaces: Au (111), Pt (111) and Ag (111)," *Top. Catal.* **60**, 503-512(2017).
[65] Y. Liu, F. Yang, Y. Zhang, J. Xiao, L. Yu, Q. Liu, Y. Ning, Z. Zhou, H. Chen, W. Huang, P. Liu, and X. Bao, "Enhanced Oxidation Resistance of Active Nanostructures *via* Dynamic Size Effect," *Nat. Commun.* **8**, 14459(2017).
[66] M. Muhler, R. Schlogl, and G. Ertl, "The Nature of the Iron Oxide-Based Catalyst for Dehydrogenation of Ethylbenzene to Styrene 2. Surface Chemistry of the Active Phase," *J. Catal.* **138**, 413(1992).
[67] R. Bliem, J. van der Hoeven, A. Zavodny, O. Gamba, J. Pavelec, P. E. de Jongh, M. Schmid, U. Diebold, and G. S. Parkinson, "An Atomic-Scale View of CO and H_2 Oxidation on a Pt/Fe_3O_4 Model Catalyst," *Angew. Chem. Int. Ed.* **54**, 13999-14002(2015).
[68] T. Fujii, F. M. F. de Groot, G. A. Sawatzky, F. C. Voogt, T. Hibma, and K. Okada, "*In situ* XPS Analysis of Various Iron Oxide Films Grown by NO_2-Assisted Molecular-Beam Epitaxy," *Phys. Rev. B* **54**, 9(1999).
[69] E. de Smit, M. M. van Schooneveld, Fabrizio. Cinquini, H. Bluhm, Phillippe. Sautet, F. M. F. de Groot, and B. M. Weckhuysen, "On the Surface Chemistry of Iron Oxides in Reactive Gas Atmospheres," *Angew. Chem. Int. Ed.* **50**, 1584-1588(2011).
[70] Z. Duan, and G. Henkelman, "Calculations of CO Oxidation over a Au/TiO_2 catalyst: A study of Active sites, Catalyst Deactivation, and Moisture Effects," *ACS Catal.* **8**, 1376-1383(2018).
[71] H. Zhong, L. Wen, J. Li, J. Xu, M. Hua and Z. Yang, "The Adsorption Behaviors of CO and H_2 on FeO Surface: A Density Functional Theory Study," *Powder Technol*. **303**, 100-108 (2016).
[72] J. Yoo, X. Rong, Y. Liu, and A. M. Kolpak, "Role of Lattice Oxygen Participation in Understanding Trends in the Oxygen Evolution Reaction on Perovskites," *ACS Catal*. **8**, 4628-4636(2018).
[73] A. Grimaud, O. Diaz-Morales, B. Han, W. T. Hong, Y. L. Lee, L. Giordano, K. A. Stoerzinger, M. T. M. Koper, and S. H. Yang, "Activating Lattice Oxygen Redox Reactions in Metal Oxides to Catalyse Oxygen Evolution," *Nat. Chem.* **9**, 457–465(2017).
[74] Z. Duan, and G. Henkelman, "Calculations of CO Oxidation over a Au/TiO_2 catalyst: A study of Active sites, Catalyst Deactivation, and Moisture Effects," *ACS Catal.* **8**, 1376-1383(2018).
[75] H. Y. Kim and G. Henkelman, "CO Oxidation at the Interface of Au Nanoclusters and the Stepped-CeO_2(111) Surface by the Mars–van Krevelen Mechanism," *J. Phys. Chem. Lett.* **4**, 216-221 (2013).
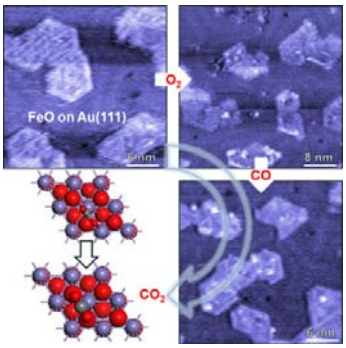
TOC Graphic